Correction: Ion Optics Model for Rapid Assessment of Gridded Ion Thruster

Performance and Life

Author(s) Name: Christopher M. Cretel, Richard E. Wirz
Author(s) Affiliations: Oregon State University, Oregon State University & Univ. of Ca. Los Angeles

Correction Notice

- Replacing the third sentence in Future Work section with "This effort introduced the idea of using the exact dynamic mode decomposition [24] to propagate grid erosion however the intermittent transients of grid erosion is not well represented by this implementation. Iterations of the DMD may still be considered and future efforts will explore the physics-informed DMD [26], which can be formulated to enforce principles such as mass conservation or the optimized DMD (OPT-DMD) [27] which utilizes the variable projection method. These approaches are not necessarily mutually exclusive, thus leading to a synthesized DMD approach." Which more appropriately cites H. Tu with the exact dynamic mode decomposition, the physics informed dmd, and cites the OPT-DMD.

  - [24] H. Tu, J., W. Rowley, C., M. Luchtenburg, D., L. Brunton, S., Nathan Kutz, J., ,Dept. of Mechanical and Aerospace Engineering, Princeton University, Princeton, NJ 08544, and ,Dept. of Applied Mathematics, University of Washington, Seattle, WA 98195, "On dynamic mode decomposition: Theory and applications," Journal of Computational Dynamics, Vol. 1, No. 2, 2014, pp.391–421. https://doi.org/10.3934/jcd.2014.1.391, URL http://aimsciences.org//article/doi/10.3934/jcd.2014.1.391
  - [26] Baddoo, P. J., Herrmann, B., McKeon, B. J., Nathan Kutz, J., and Brunton, S. L., "Physics-informed dynamic mode decomposition," Proc. R. Soc. A., Vol. 479, No. 2271, 2023, p. 20220576. https://doi.org/10.1098/rspa.2022.0576, URL https://royalsocietypublishing.org/doi/10.1098/rspa.2022.0576.
  - [27] Askham, T., and Kutz, J. N., "Variable Projection Methods for an Optimized Dynamic Mode Decomposition," SIAM Journal on Applied Dynamical Systems, Vol. 17, No. 1, 2018, pp. 380–416. https://doi.org/10.1137/M1124176, URL https://epubs.siam.org/doi/10.1137/M1124176.

- The caption in Table 4 should read "Eigenvalues that correspond to the eigen-vectors in Figure 16" not "Eigen values that correspond to the"

- In Section: Future Work, replace "Furthermore, once a method is chosen to build the Grid-ROM, we will run Monte Carlo simulations in parameter space to conduct uncertainty quantification." with "Bayesian inference may also be used as the framework for applying surrogate models to explore high resolution uncertainty propagation [28]." To give credit to authors whose work inspired this direction of analysis.

  - [28] Byrne, M. P., and Jorns, B. A., "Data-driven Models for the Effects of Background Pressure on the Operation of Hall Thrusters," 2019. URL https://pepl.engin.umich.edu/pdf/IEPC-2019-630.pdf.

Ion Optics Model for Rapid Assessment of Gridded Ion Thruster Performance and Life

Christopher M. Cretel* and Richard E. Wirz.†

Oregon State University, Corvallis, Oregon, 97331

An increased need for high-power electric propulsion has placed greater importance on understanding the mechanisms that profoundly affect thruster life and performance during ground testing. To accurately predict life-ending mechanisms of gridded ion thrusters (GITs), time dependent erosion must be well understood across a range of thruster operating conditions, non-uniformities in grid geometry and discharge plasma parameters, over the entire exit plane of the thruster. This multivariate, spatially, and temporally evolving parameter space requires reduced order modeling to efficiently evaluate thruster design and operating conditions for space missions. This effort uses the CEX2D ion thruster grid model to evaluate grid performance, erosion, and electron backstreaming across discharge ion densities over the exit plane of the NSTAR thruster for operating conditions representative of conditions seen across the exit plane profile. The reduced order models exploit the direct correlation of CEX generation to grid erosion and then changes to the grid geometry with the evolution of the EBS limit. We identify that the physics mechanisms of charge exchange may be computationally expensive, thus, the results of this modeling effort will be to develop a physics informed, reduced order models for long-duration evaluation of grid performance and life.

I. Nomenclature

A	=	linear operator matrix (DMD)
j_B	=	beamlet current (A)
k	=	number of snapshots
l_g	=	grid separation (mm)
m_r	=	number of nodes along the r axis
n_i	=	ion particle density (m^{-3})
n_o	=	neutral particle density (m^{-3})
n_z	=	number of nodes along the z axis
P	=	number of steps to predict into the future (DMD)
r_a	=	accel grid radius (mm)
r_s	=	screen grid radius (mm)
V	=	Voltage (V)
X	=	data matrix
$\mathbf{y}$	=	CEX2D output data
Γ_C	=	Carbon backsputtering, flux (m^{-2})
Γ_e	=	1-D electron flux (m^{-2})

II. Introduction

Electron backstreaming is the primary end-of-life mechanism seen in gridded ion thrusters and is strongly coupled to grid geometry as it erodes over time [1]. Experimental results demonstrate the effects of off-nominal operation of gridded ion thrusters and high fidelity models have been developed to further investigate the causes and second order phenomena of grid erosion. However, during development thrusters are operating in vacuum facilities that imperfectly mimic the space environment, thus leading to discrepancies between the models and experimental results.

---

*PhD Student, Mechanical, Industrial, and Manufacturing Engineering, AIAA Student Member.
†Boeing Professor, Executive Director of Aerospace Research Programs, Department of Engineering, AIAA Associate Fellow.

During ground testing, GITs are placed in a vacuum chamber facility with typically metallic walls and vacuum pumps capable of reaching between 1×10^{-4} to 1×10^{-6} Torr depending on thruster propellant throughput and the chamber's vacuum pumps. It has been documented that these environments alter the performance and life mechanisms of electric propulsion systems [2–4]. Gridded ion thruster are primarily affected by the remnant atmospheric gas ($n_{o,fac}$) altering behavior in the ion beam and surface sputterants (Γ_C) masking grid erosion [5]. These facility effects are expected to grow proportionally with power. NASA, therefore has established the Joint Advanced Propulsion Institute (JANUS) to enable and proliferate high power electric propulsion for deep space missions requiring high ΔV [6]. Understanding and isolating these effects and developing predictive engineering models is key to JANUS's charter and the advancement of EP devices to increasingly higher power.

Required for the proliferation of high-power EP systems is the development of integrated systems models capable of predicting life and performance of high ΔV propulsion systems. CEX2D is a high fidelity model that couples the relationship between time dependent grid erosion and electron backstreaming in gridded ion thrusters[7–9]. JANUS uses this and other models to create bespoke performance outputs for a specific thruster design and mission profile. Models are coupled to each other and independently run to produce an output. The process is iteratively repeated as thrusters are developed, but it is also inefficient. These methods do not lend themselves to the high resolution parameter exploration required for uncertainty quantification. The ultimate goal of this effort is to use the ion optics model CEX2D to develop a reduced order surrogate model to fit within the gridded ion thruster predictive engineering model (GIT-PEM) framework that is computationally efficient enough to run Monte Carlo simulations for uncertainty quantification.

III. Approach

Figure 1 shows the framework of the GIT-PEM. A mission profile is fed into three independent modules (discharge chamber, grids, and plume) which are coupled to each other through various degrees of bi-directional inputs and outputs [10]. The output is predicted life and performance of the thruster. The facility module represents the environment that the thruster is operating in and therefore feeds uncertainties into each module.
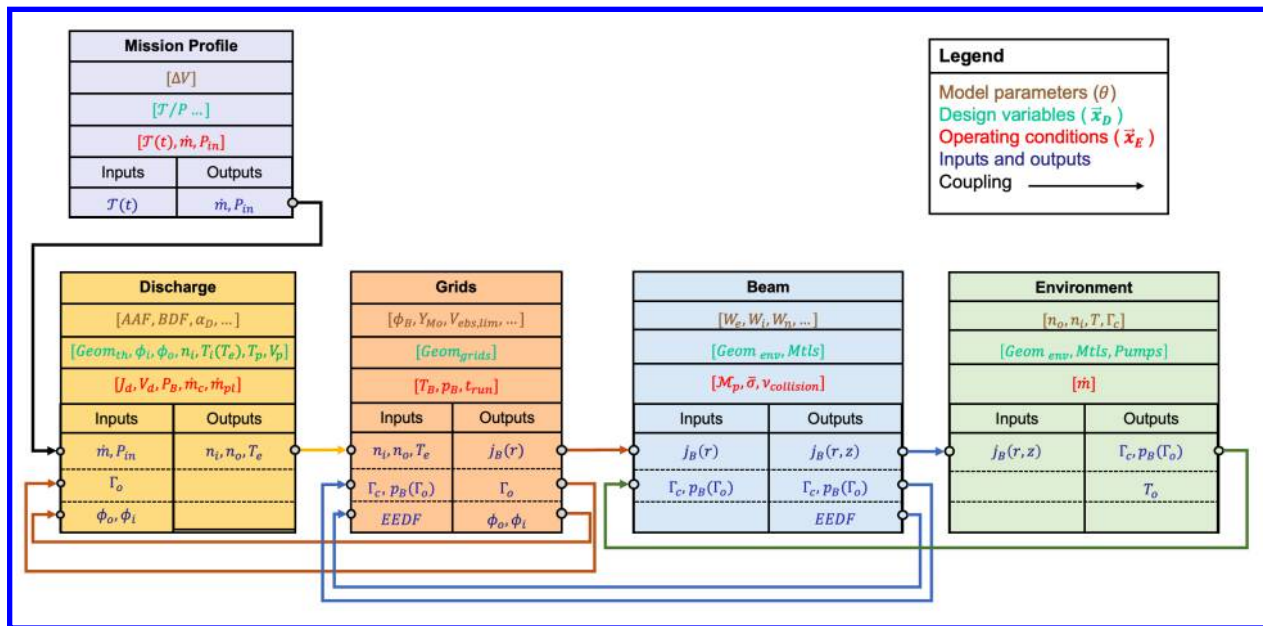

Fig. 1   GIT PEM flow chart [6, 10]

This effort exclusively looks at a reduced order model of the Grids module, currently simulated by the CEX2D code. CEX2D is an ion optics code that was developed to account for charge exchange ion behavior in a single, axisymmetric beamlet. The code is a complex series of integrated models that have been incorporated as new phenomenon have been observed in empirical data. Mass loss tracking and integration of electrons over a potential surface included in the models has narrowed the discrepancy between empirical data and modeled results [8, 9]. Thus, CEX2D is a

high-fidelity model that has proven to be consistent with empirical data, however more computational efficiency is required to integrate CEX2D into higher level systems models.
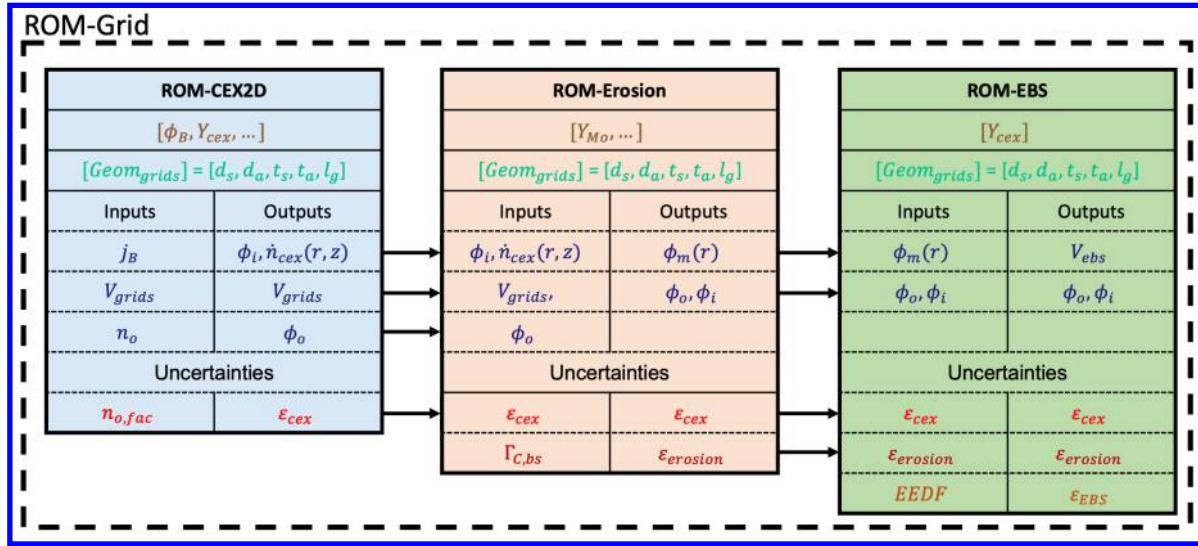

Fig. 2   The Grid model from Figure 1 is disaggregated into three unique ROMs; charge exchange ions, grid erosion, and electron backstreaming. This framework isolates environment uncertainties, $n_{o,fac}$, Γ_C, and EEDF.

Reduction in the complexity of CEX2D while maintaining a high level of accuracy is a goal of the JANUS program. Order reduction must be cautiously applied to ensure the model is bound by physical limitations while maintaining a baseline generality. A breakout of the reduced order surrogate is shown in Figure. 2 where the Grid module is further broken out into charge exchange ions (CEX), grid morphology, and electron backstreaming. This framework allows facility effects to be precisely included in the phenomena it is known to affect. For example, Figure 3 shows that the location where CEX ions are created affects the type of erosion seen on the grids [9] In Figure 2, the presence of remnant atmospheric gas in the vacuum chamber affects the rate that charge exchange ions are created [7]. Carbon re-deposition on the downstream surface of the grids masks net grid erosion [11, 12]. Electron backstreaming assumes a Maxwellian energy distribution, but the ROM should be capable of implementing other distribution models.
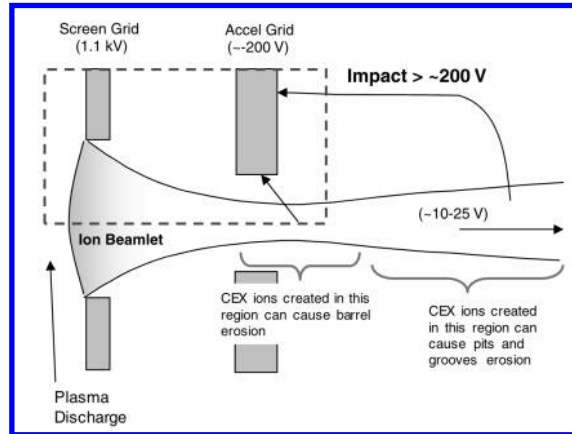

Fig. 3   Charge-exchange ion creation causes certain grid geometry changes depending on where the ion is created. Intra-grid CEX ion creation causes barrel erosion and plume region ion creation causes pits and grooves erosion [9]

The GIT-PEM ROM is developed by abstraction of computationally expensive plasma physics. Maintaining many of the same coupling parameters between modules, the ROM framework will provide inputs for uncertainty functions

known prior to running the simulation. This ultimately allows for the efficient Monte Carlo modeling for uncertainty quantification (UQ), a necessary step in the understanding of how thrusters will operate in space from empirical data taken on the ground.

Previously identified key influencing factors of time-depending electron backstreaming are isolated and fed into CEX2D to be used as the full order model (FOM). The output of the FOM then provides the data to be used as benchmarks for the assessment of order reduction methods. The data should capture first order effects of variations in the input parameters while significantly decreasing the run time compared to the FOM. The resulting ROM will represent CEX2D in the GIT-PEM framework for fast assessment of life and performance.

IV. Formulation, Results and Discussion

A. Modeling Framework

The GIT-PEM ROM's purpose is to provide a computationally efficient integrated model capable of propagating ground testing data to mission life and performance with uncertainty quantification. The JANUS effort produced the framework for the GIT-PEM shown in Figure 1. A 10 khr CEX2D simulation with electron backstreaming calculations exceeds 2 hours on a basic consumer laptop. When impingement due to near perveance conditions is modeled, the computation time can exceed 10 hours for a single run. Therefore, analysis such as uncertainty quantification will require a reduction in the computational runtime which can be achieved by the reduced order model.

A physics-based geometric representation of the ion optics was attempted to capture operational perveance limits. Perveance is a metric used assess the operating range of gridded ion thruster [13]. Perveance can be defined as the ratio $P = \frac{j_B}{V_T^{3/2}}$ which is derived from the Child-Langmuir law. However, the actual limits of operation are when beam ion trajectories impinge on the accel grid, called in this work the operational perveance limits. High perveance was geometrically simplified to an ion traversing a straight line from the upstream corner of the screen grid and just impinging on the downstream corner of the accel grid across the axis. Low perveance was similarly described by an ion traversing from the upstream corner of the screen grid but impinging on the upstream corner of the accel grid across the beamlet axis. CEX2D was used to simulate the perveance condition however due to the spatially and temporally multivariate nature of the plasma physics present in the beam, this simple analytical model was not sufficient to accurately describe life and performance. Data-driven techniques were then employed.
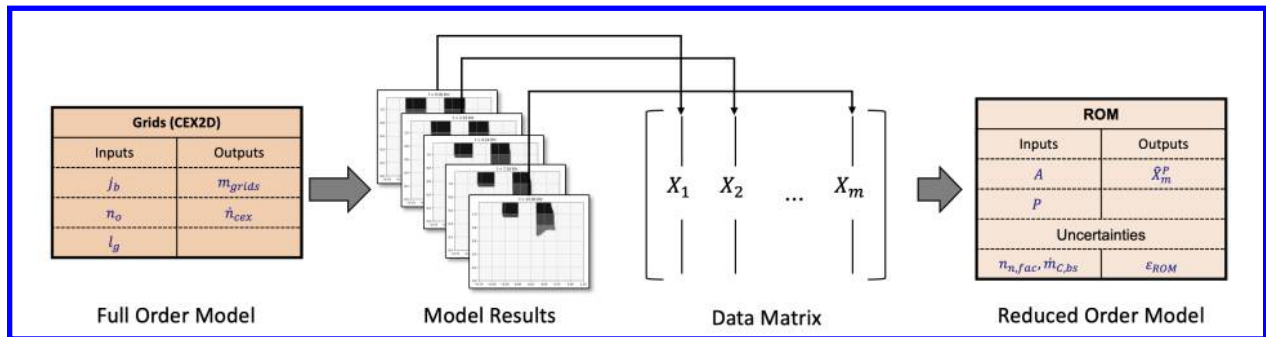

Fig. 4   GIT-PEM framework developed under the JANUS effort.

CEX2D is well suited to be replaced by a surrogate in the integrated systems level model. Figure 4 demonstrates the process of creating a reduced order model from the output data of CEX2D. CEX2D is first used to produce large quantities of data. The outputs of interest are collected and reshaped into column vectors, then re-organized into a snapshot matrix. This step can accept either time-series data such as grid evolution, or parameter-space data such as high resolution variations in upstream plasma parameter. Once the data matrix is built, it is fed into one of several data-driven analysis techniques. What results is a reduced order representation of the model results and a breakdown of inconspicuous features present in the results. The reduced order model can now be used to assess actual mission parameters of interest. The ROM box in Figure 4 is organized to represent a typical data driven method where a reduced order matrix, A and predictive steps P are used to propagate the data matrix into the future, $\hat{X}_m^P$. Uncertainties are incorporated in the bottom row, indicating that they will be carried through the model as well.

B. CEX2D Description

CEX2D is an ion optics code that accounts for CEX ion creation in its calculations. The code iteratively solves Poisson's equation for the region surrounding the grids, flows the ion beam, and recalculates Poisson's equation for the space charge effects of the ion beam [7]. CEX2D has incorporated time-dependent grid erosion into the ion optics model. The computational domain is a series of nodes assigned mass by the density of the material that resides within it. Molybdenum is used on the NSTAR FMT therefore, grid nodes are given by molybdenum's density. Vacuum nodes are assigned a mass of zero. As particles collide with grid nodes, the grid node mass is decreased according to the sputter yield [9, 14, 15]. Once a grid node's mass is depleted, it is treated like a vacuum node and the potential is recalculated. This methodology maintains the coupled relationship of grid erosion and electron backstreaming through the potential field.

In CEX2D, EBS is described by Eqn. 1. The one-sided flux of electrons adjacent to the grid is derived from the Boltzmann relation and integrated from $r = 0$ to $r = r_a$ [1].

$$I_{ebs} = e2\pi \int_0^{r_a} \Gamma_e(r)r dr = e2\pi \frac{n_{bp}\bar{c}}{4} \int_0^{r_a} \exp\left(\frac{\phi_m(r) - \phi_{bp}}{T_e}\right) r dr \tag{1}$$

Equation 1 is highlighted because of its sensitivity to two phenomenon; electron energy distribution and grid erosion. CEX2D assumes that electrons in the plume are described by a Maxwellian distribution. This assumption may be over-simplified or the distribution can take another form in the vacuum facilities and in-space operation. Dr. Levin is using the CHAOS code to model the electron energy distribution function ($EEDF$) in the plume region which will effect this calculation. Grid erosion decreases the potential barrier, ϕ_m, leading to an increase in backstreaming electrons, therefore the two phenomena are highly coupled. Experimentally, the retarding potential (ϕ_{ebs}) required to limit electron backstreaming to <1% of the beam current, is found by incrementally decreasing the accel grid voltage until a spike in current is measured from the anode, CEX2D takes the same approach to determine EBS [1].

CEX2D produces results in $n_z \times m_r$ matrices where n_z is the number of axial nodes and m_r is the number of radial nodes. For this effort n_z and m_r are 530 and 61 respectively, although these values are model parameters and can be set at run time by the operator. For outputs such as grid node mass, which evolves in time, CEX2D outputs k snapshots of $(n_z \times m_r)_t$ matrices corresponding to the grid node mass at time t. This is denoted as $\mathbf{y}^k = [\bar{y}_0, \bar{y}_1, \bar{y}_2, ...\bar{y}_k]$ where $\bar{y}_i \in \mathbb{R}^{1 \times n_z m_r}$. Note that the individual snapshots are reshaped into column vectors of $n_r m_z$ elements. Typically, $k \ll n_r m_z$ making the resulting $\mathbf{y}^k$ matrix tall and skinny.

C. Simulation Inputs

The NASA Solar Technology Readiness (NSTAR) flight model thruster (FMT) was developed for NASA's Deep Space mission to demonstrate advanced propulsion technologies for missions requiring high ΔV. It is presented as a benchmark for GIT modeling. The NSTAR FMT has been extensively tested to understand neutral density, ion density, and grid separation which provides useful inputs to CEX2D [16, 17]. CEX2D was a key tool in analyzing the NSTAR thruster and showed good agreement with experimental results [8, 12]. Table 1 presents the grid geometry used to represent the NSTAR FMT and table 2 shows the nominal operating conditions for the TH15, TH8, and TH0 throttle conditions representing high, medium, and low thrust operation.

Table 1   NSTAR nominal thruster geometries [18]

d_s (mm)	d_a (mm)	t_s (mm)	t_a (mm)	l_g cold,hot (mm)
1.91	1.140	0.381	0.381	0.66, 0.36

Table 2   Three nominal NSTAR operating set points.

Throttle Point	V_a (V)	V_D (V)	V_B (V)	J_b (A)	V_{space} (V)
TH15	-180	26	1110	1.76^{-4}	25
TH8	-180	26	1110	7.00^{-5}	25
TH0	-150	26	650	3.00^{-5}	25

5

Modeling the NSTAR FMT requires near-mission operating parameters to create useful results. The inputs of this effort are informed by the neutral density measurements of the discharge chamber measured in [16] and the grid separation measurements in [17]. In [16], neutral density was measured by probing the discharge plasma because peripheral neutral depletion was suspected of causing causing performance degradation off axis of the grids. The effort also measured electron temperature and density which provided insight into ion density adjacent to the grids for this effort.

In [17], grid separation was measured while the thruster was operating. A ceramic pin was fixed to the screen grid and fed through a concentric accel gridlet. A long distance microscope and image processing software then measured variations in the height of the pin above the accel grid to measure the change in spacing between the grids. Neutral density, ion density, and grid separation have demonstrated radial trends across the thruster face which leads to non-uniform variations of grid erosion and electron backstreaming. Table 3 presents the trials used to explore the parameter variations in this study.

Table 3   The trials studied represent a range of operating conditions that encompass nominal and off-nominal conditions for the NSTAR FMT.

Trial	Parameter	Value [A]	Trial	Parameter	Value [mm]	Trial	Parameter	Value [m^{-3}]
F1	j_B	1.76×10^{-4}	G1	l_g	0.36	H1	n_n	2.51×10^{18}
F2	j_B	1.179×10^{-4}	G4	l_g	0.66	H2	n_n	3.77×10^{18}
F3	j_B	2.64×10^{-4}	G6	l_g	0.16	H3	n_n	6.28×10^{18}

CEX2D is used to model variations in beam current, neutral density, and grid separation shown to occur across the radial profile of the NSTAR FMT. Trials are simulated for 10 khrs. In Figures 5, 7, and 7, the creation rate of CEX ions is plotted with ion trajectories. A correlation is clearly apparent between the parameter of interest, j_b, l_g and n_o and the creation rates and location of CEX ions. Previous works have identified that CEX ions are a leading cause of grid erosion [7, 9]. The magnitude of CEX ion creation coincides with grid erosion rate and the location of CEX ions correlate with how geometric feature form over time due to erosion.
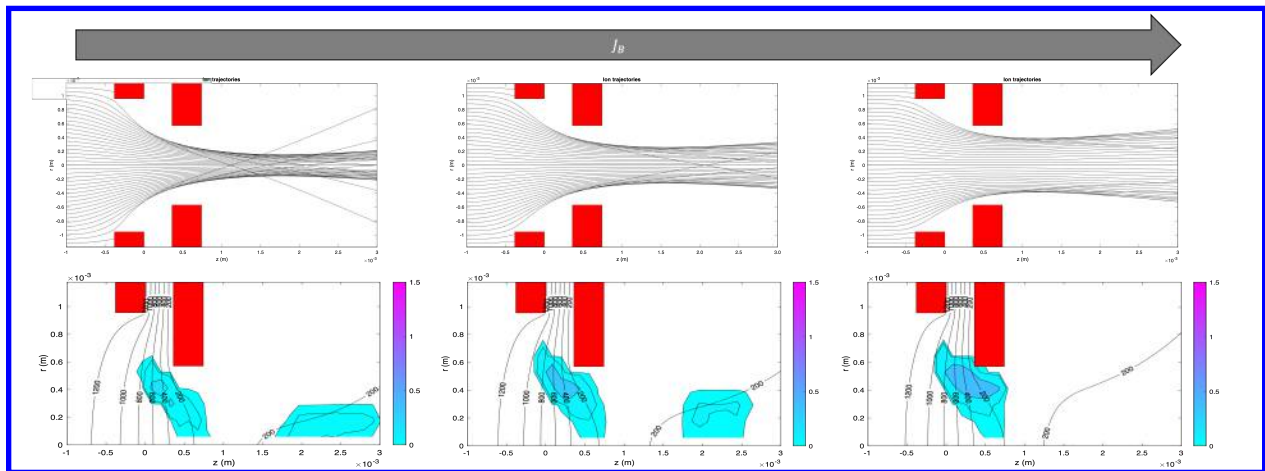

Fig. 5   Charge exchange ion creation rates for trials F2, F1, and F3 approaches the accel grid with increasing j_b
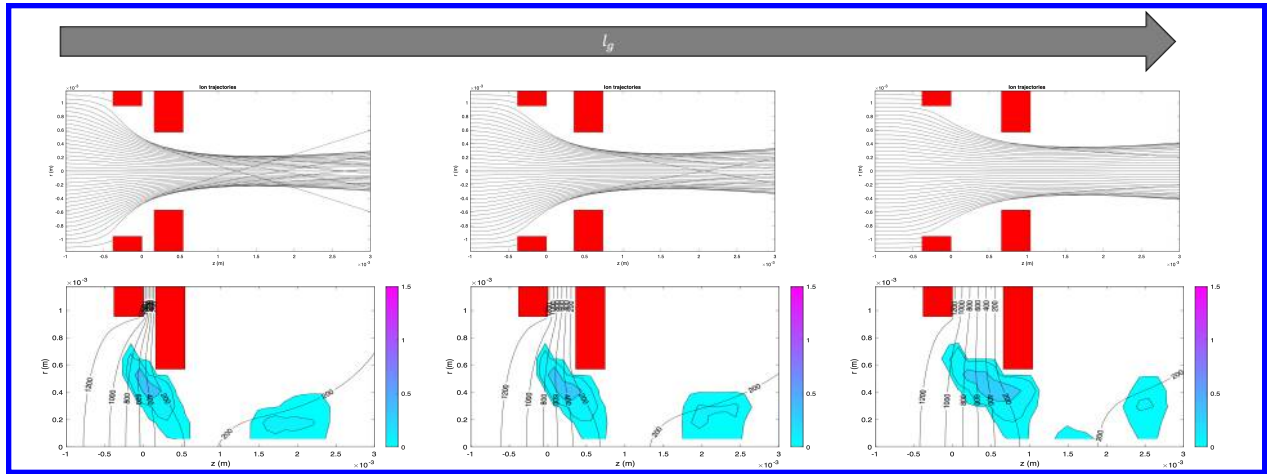
6

Fig. 6   From left to right, trials G6, G1, and G4 are shown. As the intra-grid region expands, more charge exchange ion are created between the grids.
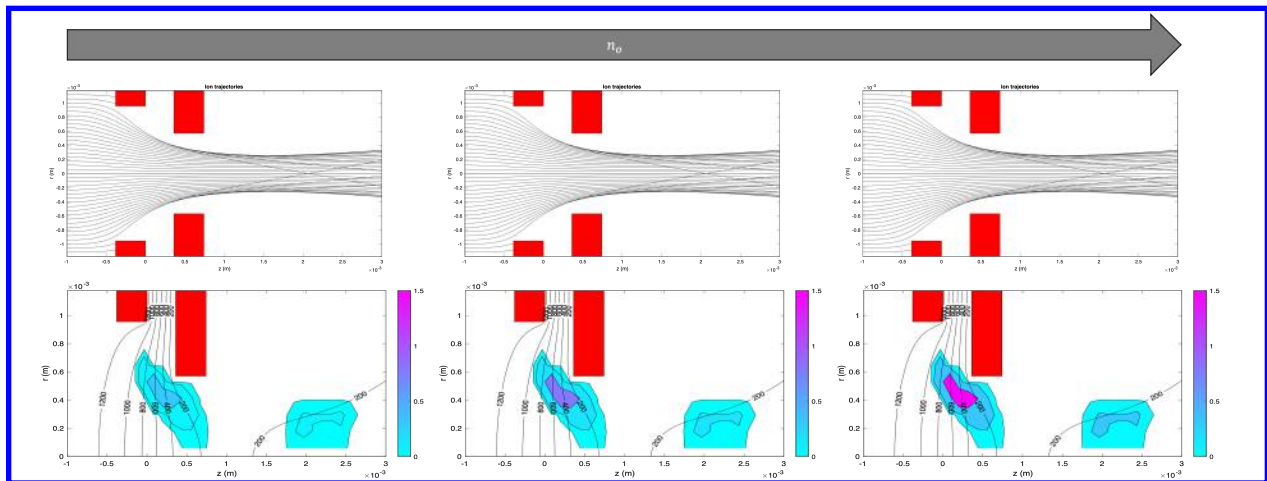

Fig. 7   From left to right, trials H1, H2, and H3 are shown. Neutral density (n_o) has no effect on the location that charge exchange ions are created, but shows a significant increase in creation rates.

Figure 8 shows the total mass loss for the parameters of interest. The values plotted exceed the domain of Table 3 to highlight trends and the NSTAR FMT nominal parameters are highlighted. Total mass loss of the grids is dependent on j_b and n_o while very subtly dependent on l_g. High correlations can be used to easily identify grid erosion features for analysis, so the remainder of this section, the F trials will be the focus.
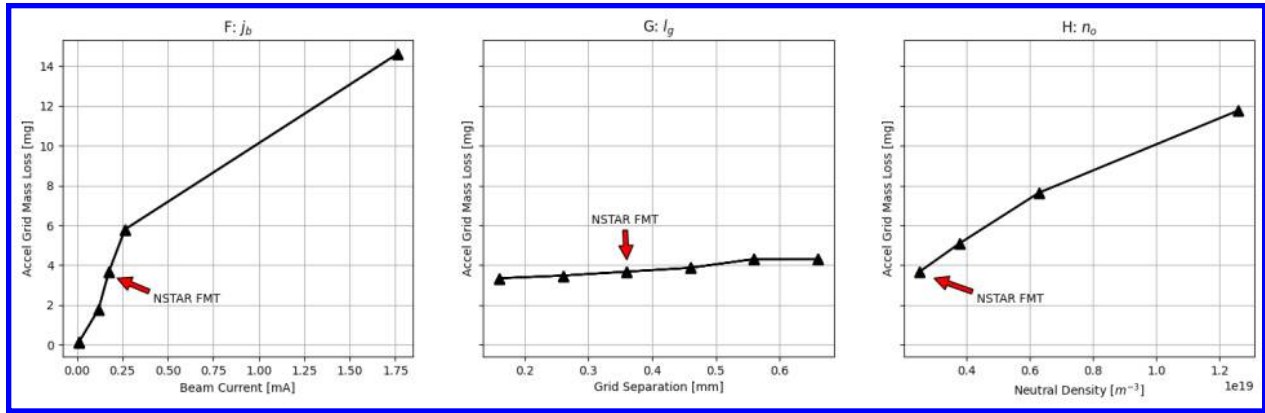
7

Fig. 8   Total mass loss of each family of trails. Mass loss is most strong correlated by the beam current and only weakly correlated with grid separation.

Figure 9 demonstrates the effect beamlet current has on grid evolution due to CEX ion bombardment erosion. The trials plotted are those from Table 3 at $t = 0$, $t \approx 5$ and $t = 10$ khrs. For the lowest beamlet current, erosion is only prevalent on the downstream corner known as chamfering. For the nominal NSTAR operating set point (middle) barrel erosion and downstream chamfer erosion seem to be occurring simultaneously, however the minimum aperture diameter has not changed much. The highest beamlet current shows significantly more reduction in minimum aperture diameter between $t = 0$ and $t = 5$ khrs. From $t = 5$ to $t = 10$ khrs, the downstream half of the aperture erodes much more quickly than upstream half. Chamfer erosion has been shown to contribute to increased electron backstreaming, even when the minimum aperture diameter has not changed much.
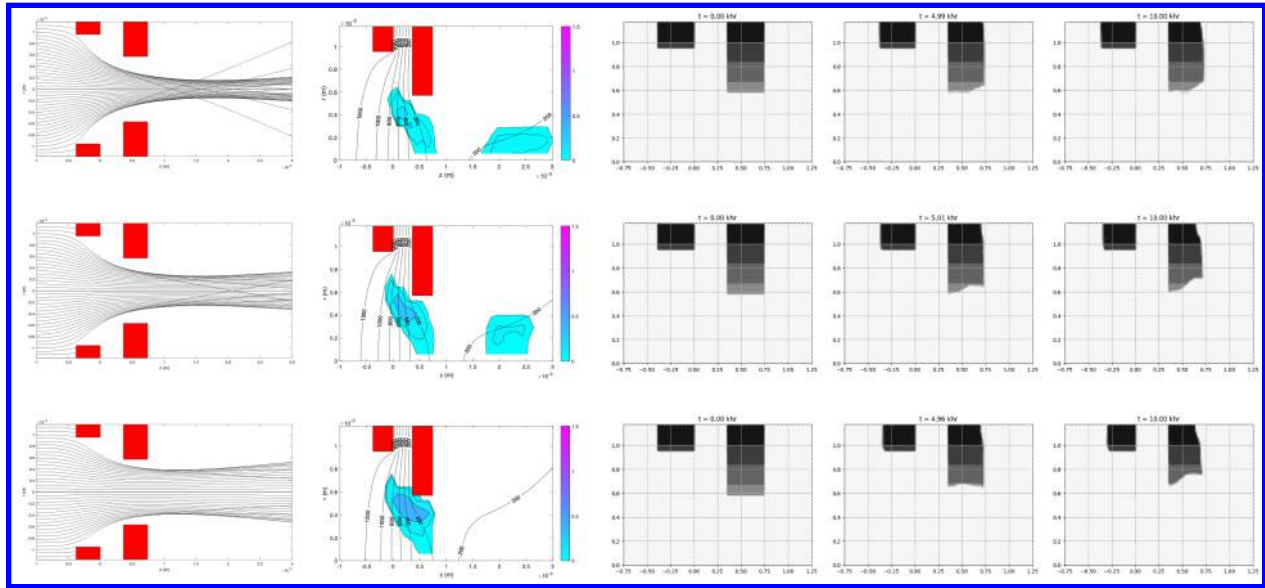

Fig. 9   CEX ion profiles cause unique grid erosion patterns to evolve over time.

The purpose of the GIT-PEM is to have a computationally efficient way to investigate life and performance of gridded ion thrusters. The features presented in Figure 9 require further investigation and a qualitative way to describe the erosion phenomena happening due to CEX ion bombardment. Analytically, this would be a daunting challenge as CEX ion creation and grid erosion are stochastic processes. In the next section, we identify that data-driven techniques are well suited address this challenge.

CEX2D does not output grid node mass at predetermined uniform time steps. For some analysis, this is not a challenge, but for others this can introduce noise when applying an order reduction technique to the data. Figure 10

demonstrates the non-uniformity of the time steps for trial F3 in Table 3. Interpolation is used used to create uniformly distributed $\hat{k}$ snapshots at the cost of introducing uncertainty due to the extra calculation.
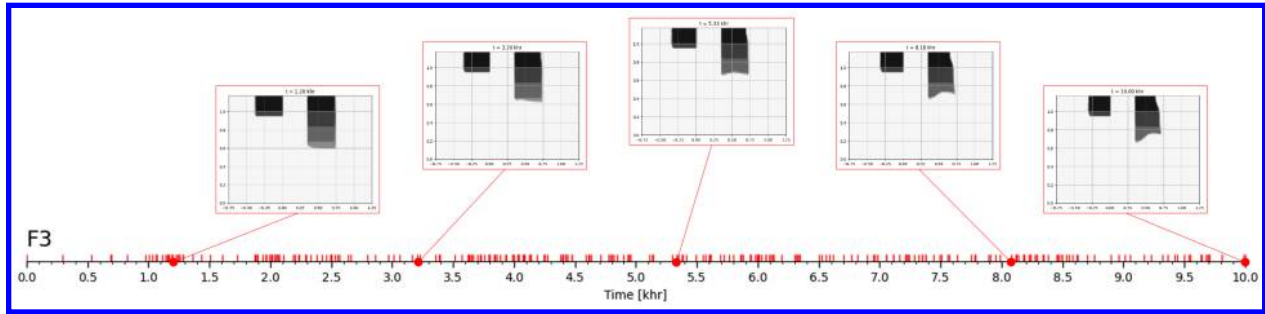

Fig. 10   CEX2D timestep distribution for trial F3.

D. Exploration of Data-Driven Techniques

Data-driven techniques are explored to determine the best method for creating the Grid-ROM from Figure 2. Many of these techniques have been developed for facial recognition and fluid flow analysis. This effort identifies that grid erosion can be characterized somewhere between static images of grids with discrete geometric variations similar to faces in [19] and dynamic time-series of grid evolution, similar to flow fields in [20]. Therefore, there may not be one technique that entirely meets the needs for parameter-space exploration and predictive evolution of grid erosion. The two techniques that capture the bounds of the parameter space we wish to explore are the singular value decomposition (SVD) and the dynamic mode decomposition (DMD). For both the SVD and the DMD, a data matrix, X will be presented. The specifics of this matrix depends on the technique employed and the parameters being investigated.

The singular value decomposition is one of the most significant decomposition methods in linear algebra and data-science. The analysis of end-of-life grid erosion will follow the eigen-face method in [21]. This procedure can be used to compress the storage of large grid erosion data sets as well as utilize classification methods for determining input parameters. To analyze the parameter space using the SVD, the data matrix X can be built by extracting grid node mass data at a predetermined snapshot over many trials that vary the parameter of interest. For example, this effort extracts the final grid node mass matrix from trials F1 through F3 and H1 through H3. The dimensions of X are then 6×32330.

To analyze the X matrix, first step is plotting the singular values, σ_i and the cumulative sum of the singular values. This provides a visual representation of the significance of each eigen-image and how many of those eigen-images are required to minimize the truncation error. Next, some pre-determined number of columns, r, of U are plotted to analyze the elements of the most significant r eigen-images. To analyze the principle components, take the mean of the columns of X and apply the SVD to the mean-subtracted matrix [19].

The dynamic mode decomposition extracts dynamic information from flow fields generated by empirical measurements or numerical simulations [20]. The DMD assumes the existence of a linear operator A that maps the current snapshot to the next snapshot in time, $x_{t+1} = Ax_t$. The goal of the DMD is to calculate the *dynamic modes* that arise as a result of the evolution of the columns in X. The SVD is used to efficiently calculate the psuedoinverse of the linear operator A. And in depth description of the dynamic mode decomposition can be found in [20, 22, 23].

In the original description of the DMD, the columns of the data matrix X must be uniformly spaced, sequential, time-series data. A relaxation of this requirement has been made in a redefinition of the DMD, known as the exact-DMD [23]. However, it is of little consequence to create a representative data matrix using interpolation to meet this requirement. The resulting modes found by applying the DMD represent dynamic structures that contribute to the evolution captured by the data [22]. Plotting the eigenvalues of A in the complex plane describe the time evolution of the corresponding dynamic mode. When plotted in the complex plane, eigenvalues outside the unit circle are growing in time and eigenvalues inside the unit circle are decaying.

The singular value decomposition and the dynamic mode decomposition are used to analyze grid erosion data as a result of simulating the input parameters from Tables 1, 2, and 3 using CEX2D. The analysis supports determining the order reduction methods that are most appropriate to be used in developing the GIT-PEM Grid-ROM from Figure 2. The SVD is a chosen candidate because it is the foundation for many other methods such as the aforementioned DMD, it allows for the storage of large datasets by references a subset of eigen-images, and provides a basis for classification

methods. The DMD method is a chosen candidate because of its proposed ability to extrapolate to future time-steps, isolation of dynamic phenomena, and data-source agnosticism [20, 24].

E. Data Preprocessing

The CEX2D-generated grid node mass data is given by k snapshots, denoted as $\mathbf{y}^k = [\bar{y}_0, \bar{y}_1, \bar{y}_2, ... \bar{y}_k]$ where $\bar{y}_i \in \mathbb{R}^{1 \times n_z m_r}$. A limitation of CEX2D is that it does not output uniformly spaced snapshots. Therefore, CEX2D output data is preprocessed to ensure interpretability in the SVD and DMD. Data is normalized such that the an untouched grid node holds a value of 1 and a vacuum node holds a value of 0. For the DMD, the column space is interpolated to create uniform time steps.

F. Parameter Space

The parameter space for F and H trials is investigated using the SVD. The final grid geometry for each of the trials is gathered to make a unique data matrix $X_{svd} \in \mathbb{R}^{6 \times 32330}$. The mean image of the grid node data is calculated (Figure 12) and subtracted from each of the column entries (Figure 12). The SVD is applied to the mean subtracted matrix, $X' = X_{svd} - <X_{svd}>$. This procedure is akin to finding the principle components of the data matrix X_{svd}.
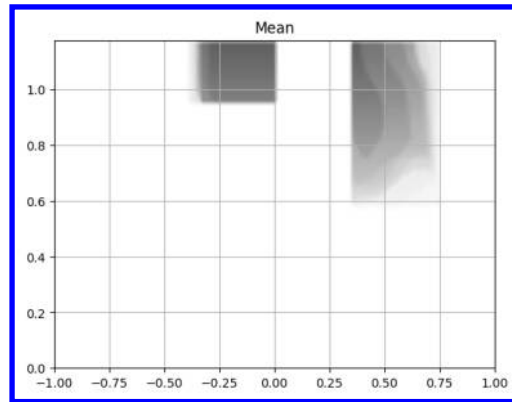

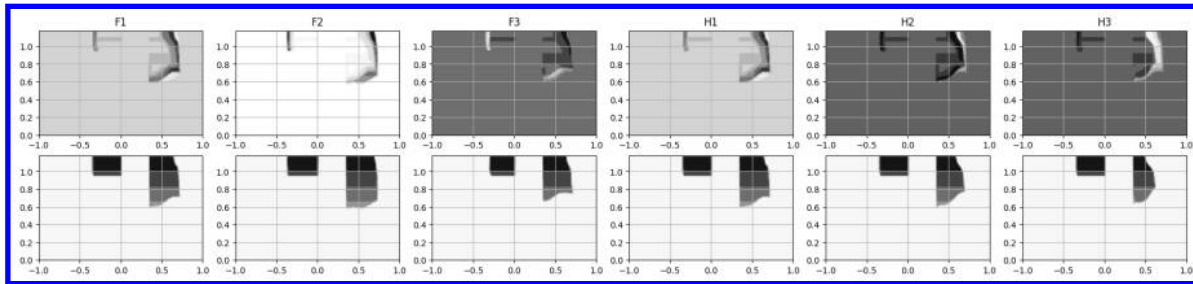**Fig. 11   Mean grid geometry for trials F1, F2, F3, H1, H2, and H3 after the thruster is operated for 10 khrs**

Fig. 12   (top) Mean-subtracted entries in the column-space of matrix X. (bottom) Entries of the column space matrix, X_{svd}

Next, the singular values are plotted in Figure 13 with the eigen-images in Figure 14. Having access to the eigen-images offers a few advantages. A subset of eigen-images can be used to classify any grid geometry given a few numbers that can be correlated to input parameters [19]. The eigen-images also form the basis for which classification methods can be applied to identify input plasma parameters from specific geometry features of the grid nodes [21].
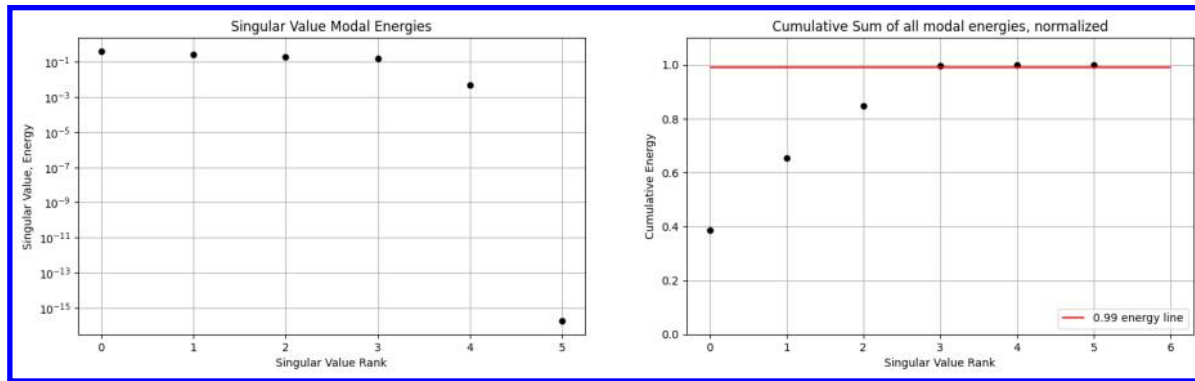
Fig. 13 **(left)Singular values are plotted in order of significance showing the range that singular values encompass. (right) The cumulative sum of the singular values are plotted where those above the threshold line can be discarded while maintaing 99% of the singular value energy**
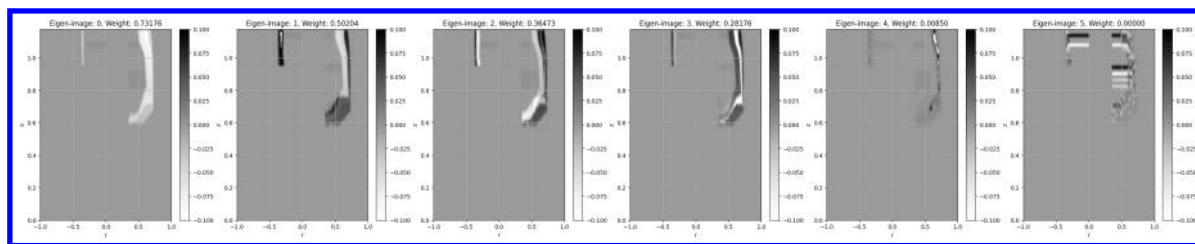

Fig. 14 **Eigen-grids isolate features of the data set that can then be used for the basis in classification methods.**

The data-set used in this exercise is notably small, only 6 grid samples are used varying only two parameters, but is presented as an initial demonstration of the methodologies and objectives described above. To appropriately apply this method, we would want to gather samples over many more input parameters. Future work in applying this technique will vary each parameter with upwards of 50 unique values and expand the number of parameters explored to a dataset representative of the design space of gridded ion thrusters. Fortunately, the process does not change considerable for 6 entries or 1000 entries.

An attempt was made to apply the DMD to the trial G3. In this test, the evolution of grid geometry was explored from $t = 0$ to $t = 10 khrs$. First, the data was interpolated to create uniformly space time-series data matrix, X_{dmd}. We used $\Delta t = 0.05$ khrs to create 201 snapshot. The singular values were calculated to determine the rank reduction appropriate to maintain 99% of the information held in X_{dmd}.
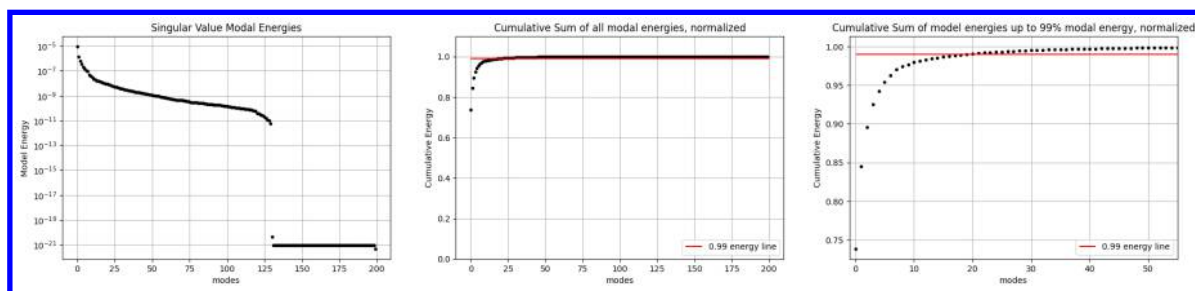

Fig. 15 **(left) Singular values are plotted with decreasing weight, and (middle) plotted against the threshold required to achieve the above 99% threshold used in this study**

Figure 15 demonstrates the range of singular values. Rank reduction is achieved by only keeping the values above the threshold line (red) corresponding to 99% of the cumulative energy. This amounts to more than a 90% reduction in data necessary to capture most of the dynamics present in the snapshots.
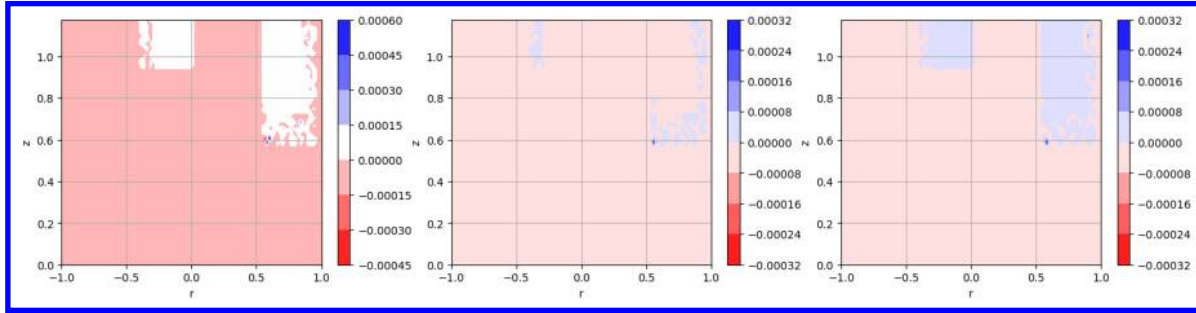
11

Fig. 16   The first three eigen-vectors of the linear operator matrix, A are plotted as a resulf to applying the DMD to trial G3

Table 4   Eigen values that correspond to the

λ_1	λ_2	λ_3
$8.95 + 0j$	$6.86 + 5.76j$	$6.86 - 5.76j$

After the linear operator matrix, A is calculated, the eigenvectors of A are plotted to produce eigen-grids which are the spatial modes governing the evolution of the grids by erosion. The eigen-grids are plotted in Figure 16. These can be paired with the time-dynamics described by the complex numbers in Table 4 to diagnose the phenomena as grid geometry evolves in time. These can also be used to predict the future state of the grid geometry which would be useful for extending simulation domains. Finally, Figure 17 is another way to present the eigen-values of the A matrix. Values that lie inside the unit circle, plotted in black, decay in time, while the opposite is true for values that lie outside the unit circle.
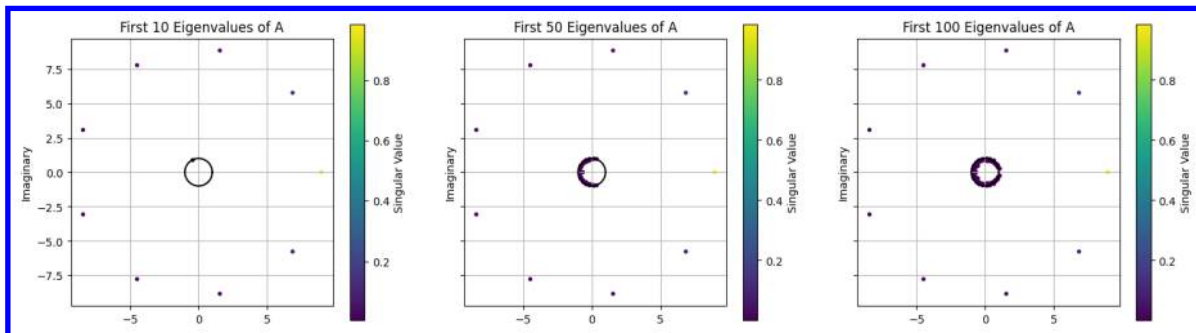

Fig. 17   The eigenvalues of A are plotted in the complex plane where values inside the unit circle decay and values outside grow in time

While most of the values lie on the unit circle, those that correspond to the most significant modes are well beyond it, meaning they are growing significantly within this simulation.. These values will be further investigated in future work. It is expected that the results presented herein are not necessarily accurate because physics constraints such as mass conservation is ignored. However, what these results show is the process for utilizing the SVD and DMD for grid erosion analysis.

V. Conclusion

This effort introduces the framework for developing a reduced order grid model based on the successful ion optics model CEX2D. Where CEX2D coalesces the charge exchange, grid erosion, and electron backstreaming model, the Grid-ROM dissociates them in order to isolate the inclusion of uncertainties related to test facility effects and differences in the thruster's environment. Through this method, the effects of background neutral density, carbon backsputter and the EEDF on thruster life and performance can be explored independently, saving computation time and allowing

12

isolated analysis of uncertainties and sensitivities. Preliminary analysis of the output data provided by CEX2D shows that it is well suited to provide entries into the data matrices necessary to apply the singular value decomposition and methods such as the dynamic mode decomposition. This method can be applied to efforts in electric propulsion life and performance analysis where sufficient data through experiments and/or validated models are available.

VI. Future Work

Analyzing CEX2D results and processing and exploring data-driven methods, allowed the formulation of approaches to apply techniques used in fields such as facial recognition and computational fluid mechanics. The data used herein was a small subset of the available data that CEX2D has produced, so gathering and preprocessing the remaining data will provide higher resolution and better results. This effort introduced the idea of using the dynamic mode decomposition to propagate grid erosion, while future efforts will explore the physics-informed DMD [25], which can be formulated to enforce principles such as mass conservation to the calculation of the linear operator matrix and better reflect the physics relevant processes such as grid erosion. Furthermore, once a method is chosen to build the Grid-ROM, we will run Monte Carlo simulations in parameter space to conduct uncertainty quantification. With uncertainty quantification and confidence in the ROM, we will integrate with the other models to form the overall GIT-PEM for predictive evaluation of ion thruster life and performance.

VII. Acknowledgements

References

[1] Wirz, R. E., Katz, I., Goebel, D. M., and Anderson, J. R., "Electron backstreaming determination for ion thrusters," *Journal of Propulsion and Power*, Vol. 27, No. 1, 2011, pp. 206–210. https://doi.org/10.2514/1.46844, publisher: American Institute of Aeronautics and Astronautics Inc.

[2] Randolph, T., Kim, V., Kaufman, H., Kozubsky, K., Zhurin, V., and Day, M., "FACILITY EFFECTS ON STATIONARY PLASMA THRUSTER TESTING," 1993.

[3] Soulas, G. C., "The Impact of Back-sputtered Carbon on the Accelerator Grid Wear Rates of the NEXT and NSTAR Ion Thrusters," Washington DC, USA, 2013. URL https://ntrs.nasa.gov/api/citations/20150021367/downloads/20150021367.pdf.

[4] Soulas, G. C., "Modeling Neutral Densities Downstream of a Gridded Ion Thruster," 2010.

[5] Sovey, J., and Patterson, M., "Ion beam sputtering in electric propulsion facilities," *27th Joint Propulsion Conference*, American Institute of Aeronautics and Astronautics, Sacramento,CA,U.S.A., 1991. https://doi.org/10.2514/6.1991-2117, URL https://arc.aiaa.org/doi/10.2514/6.1991-2117.

[6] Walker, M. L. R., Lev, D., Saeedifard, M., Jorns, B., Foster, J., Gallimore, A. D., Gorodetsky, A., Rovey, J., Chew, H. B., Levin, D., Williams, J. D., Yalin, A., Wirz, R. E., Marian, J., Boyd, I., Hara, K., and Lemmer, K. M., "Overview of the Joint AdvaNced PropUlsion InStitute," Boston, 2022. URL https://www.alexgorodetsky.com/static/papers/IEPC-2022-156-JANUS.pdf.

[7] Brophy, J. R., Katz, I., Polk, J. E., and Anderson, J., "Numerical Simulations of Ion Thruster Accelerator Grid Erosion," *38th AIAA/ASME/SAE/ASEE Joint Propulsion Conference & Exhibit*, American Institute of Aeronautics and Astronautics, Indianapolis, Indiana, 2002. https://doi.org/10.2514/6.2002-4261, URL http://arc.aiaa.org/doi/abs/10.2514/6.2002-4261.

[8] Wirz, R. E., "Coupled Analysis of Ion Thruster Grid Erosion and Electron Backstreaming," 2010.

[9] Wirz, R. E., Anderson, J. R., and Katz, I., "Time-dependent erosion of ion optics," *Journal of Propulsion and Power*, Vol. 27, No. 1, 2011, pp. 211–217. https://doi.org/10.2514/1.46845, publisher: American Institute of Aeronautics and Astronautics Inc.

[10] Wirz, R. E., Gorodetsky, A., Jorns, B., and Walker, M. L. R., "Predictive Engineering Model for Life and Performance Assessment of High-Power Electric Propulsion Systems," 2022. URL https://hpepl.ae.gatech.edu/sites/default/files/files/Wirz_IEPC-2022-410_PEM.pdf.

[11] Anderson, J., Sengupta, A., and Brophy, J., "Post-Test Analysis of the Deep Space 1 Spare Flight Thruster Ion Optics," *40th AIAA/ASME/SAE/ASEE Joint Propulsion Conference and Exhibit*, American Institute of Aeronautics and Astronautics, Fort Lauderdale, Florida, 2004. https://doi.org/10.2514/6.2004-3610, URL https://arc.aiaa.org/doi/10.2514/6.2004-3610.

[12] Polk, J., Chaplin, V., Yim, J., Soulas, G., Williams, G., and Shastry, R., "Modeling Grid Erosion in the NEXT Ion Thruster Using the CEX2D and CEX3D Codes," 2022. https://doi.org/10.21203/rs.3.rs-1517801/v1, URL https://www.researchsquare.com/article/rs-1517801/v1.

[13] Aston, G., Kaufman, H. R., and Wilbur, P. J., "Ion beam divergence characteristics of two-grid accelerator systems," *AIAA Journal*, Vol. 16, No. 5, 1978, pp. 516–524. https://doi.org/10.2514/3.7538, URL https://arc.aiaa.org/doi/10.2514/3.7538.

[14] Doerner, R. P., Whyte, D. G., and Goebel, D. M., "Sputtering yield measurements during low energy xenon plasma bombardment," *Journal of Applied Physics*, Vol. 93, No. 9, 2003, pp. 5816–5823. https://doi.org/10.1063/1.1566474, URL https://pubs.aip.org/jap/article/93/9/5816/779833/Sputtering-yield-measurements-during-low-energy.

[15] Rosenberg, D., and Wehner, G. K., "Sputtering Yields for Low Energy He+-, Kr+-, and Xe+-Ion Bombardment," *Journal of Applied Physics*, Vol. 33, No. 5, 1962, pp. 1842–1845. https://doi.org/10.1063/1.1728843, URL https://pubs.aip.org/jap/article/33/5/1842/164073/Sputtering-Yields-for-Low-Energy-He-Kr-and-Xe-Ion.

[16] Sengupta, A., Goebel, D., and Owens, A., "Neutral Density Measurements in an NSTAR Ion Thruster," 2006. URL https://access.library.oregonstate.edu/pdf/1330010.pdf.

[17] Diaz, E. M., and Soulas, G. C., "Grid Gap Measurement for an NSTAR Ion Thruster," 2006.

[18] Patterson, M. J., Haag, T. W., and Rawlin, V. K., "NASA 30 em Ion Thruster Development Status," 1994.

[19] Sirovich, L., and Kirby, M., "Low-dimensional procedure for the characterization of human faces," *J. Opt. Soc. Am. A*, Vol. 4, No. 3, 1987, p. 519. https://doi.org/10.1364/JOSAA.4.000519, URL https://opg.optica.org/abstract.cfm?URI=josaa-4-3-519.

[20] Schmid, P. J., "Dynamic mode decomposition of numerical and experimental data," *J. Fluid Mech.*, Vol. 656, 2010, pp. 5–28. https://doi.org/10.1017/S0022112010001217, URL https://www.cambridge.org/core/product/identifier/S0022112010001217/type/journal_article.

[21] Brunton, S. L., and Kutz, N. J., *Data-Driven Science and Engineering*, 2nd ed., 2021. URL https://faculty.washington.edu/sbrunton/DataBookV2.pdf.

[22] Schmid, P. J., and Pust, O., "Applications of the dynamic mode decomposition," *Theoretical and Computational Fluid Dynamics*, 2010. URL https://www.researchgate.net/profile/Peter-Schmid-5/publication/225152662_Applications_of_the_dynamic_mode_decomposition/links/54f1a3be0cf2f9e34efec6a2/Applications-of-the-dynamic-mode-decomposition.pdf?origin=publication_detail.

[23] H. Tu, J., W. Rowley, C., M. Luchtenburg, D., L. Brunton, S., Nathan Kutz, J., ,Dept. of Mechanical and Aerospace Engineering, Princeton University, Princeton, NJ 08544, and ,Dept. of Applied Mathematics, University of Washington, Seattle, WA 98195, "On dynamic mode decomposition: Theory and applications," *Journal of Computational Dynamics*, Vol. 1, No. 2, 2014, pp. 391–421. https://doi.org/10.3934/jcd.2014.1.391, URL http://aimsciences.org//article/doi/10.3934/jcd.2014.1.391.

[24] Hajisharifi, A., Girfoglio, M., Quaini, A., and Rozza, G., "A comparison of data-driven reduced order models for the simulation of mesoscale atmospheric flow," 2023.

[25] Baddoo, P. J., Herrmann, B., McKeon, B. J., Nathan Kutz, J., and Brunton, S. L., "Physics-informed dynamic mode decomposition," *Proc. R. Soc. A.*, Vol. 479, No. 2271, 2023, p. 20220576. https://doi.org/10.1098/rspa.2022.0576, URL https://royalsocietypublishing.org/doi/10.1098/rspa.2022.0576.